UNIVERSITY OF CALIFORNIA

Santa Barbara

# Investigation of the Seismic Nucleation Phase of Large Earthquakes Using Broadband Teleseismic Data

A Thesis submitted in partial satisfaction of the requirements for the degree of Master of Science in Geophysics

by

Eryn Therese Burkhart

Committee in charge:

Professor Chen Ji

Professor Ralph Archuleta

Professor Frank Spera

December 2014

The thesis of Eryn Therese Burkhart is approved.

Chen Ji, Committee Chair

Ralph Archuleta

Frank Spera

September 2014

## Acknowledgments

I would like to thank my advisor Chen Ji, as well as the rest of the Earth Science Faculty at UCSB. Specifically I would like to thank my geophysics professors, Ralph Archuleta and Toshiro Tanimoto. I'd also like to thank Professor Frank Spera for his support during my time as a graduate student. I'd like to thank my fellow geophysics graduate students, Jorge Crempien, Xiangu Li, Guangfu Shao, Qiming Liu, Stephanie Tsang, Luyuan Ding, and Tomoko Yano. My time at UCSB has been extraordinary and I have learned so much.

# Abstract

Investigation of the Seismic Nucleation Phase of Large Earthquakes Using Broadband Teleseismic Data

by

Eryn Therese Burkhart

The dynamic motion of an earthquake begins abruptly, but is often initiated by a short interval of weak motion called the seismic nucleation phase (SNP). *Ellsworth and Beroza* [1995, 1996] concluded that the SNP was detectable in near-source records of 48 earthquakes with moment magnitude (Mw), ranging from 1.1 to 8.1. They found that the SNP accounted for approximately 0.5% of the total moment and 1/6 of the duration of the earthquake. *Ji et al* [2010] investigated the SNP of 19 earthquakes with Mw greater than 8.0 using teleseismic broadband data. This study concluded that roughly half of the earthquakes had detectable SNPs, inconsistent with the findings of *Ellsworth* and *Beroza* [1995]. Here 69 earthquakes of Mw 7.5-8.0 from 1994 to 2011 are further examined. The SNP is clearly detectable using teleseismic data in 32 events, with 35 events showing no nucleation phase, and 2 events had insufficient data to perform stacking, consistent with the previous analysis. Our study also reveals that the percentage of the SNP events is correlated with the focal mechanism and hypocenter depths. Strike-slip earthquakes are more likely to exhibit a clear SNP than normal or thrust earthquakes. Eleven of 14 strike-slip earthquakes (78.6%) have detectable NSPs. In contrast, only 16 of 40 (40%) thrust earthquakes have detectable SNPs. This percentage also became smaller for deep events (33% for events with hypocenter depth>250 km). To understand why certain thrust

earthquakes have a visible SNP, we examined the sediment thickness, age, and angle of the subducting plate of all thrust earthquakes in the study. We found that thrust events with shallow (<50 km) hypocenters with thick seafloor sediments (>600 m) on the subducting plate tend to have clear SNPs. If the SNP can be better understood in the future, it may help seismologists better understand the rupture dynamics of large earthquakes. Potential applications of this work could attempt to predict the magnitude of an earthquake seconds before it begins by measuring the SNP, vastly improving earthquake Early Warning Systems for populated areas.

# Table of Contents

# I. Introduction

The possibility of knowing the size of an earthquake as early as possible has been an area of interest for seismologists. Of course, knowing ahead of time when and where a large earthquake will occur is not currently (nor might it ever be) possible with great precision. Certain fault zones have fairly consistent periods of rupture, so events can be predicted within years or tens of years in those cases (e.g., the Parkfield, California events of magnitude (M) ~6.0 occur roughly every 22 years.) But for the most part, until the rupture begins, we cannot say when or where an earthquake will take place. Once an earthquake begins, the calculations needed to determine the earthquake's magnitude and precise location require recording and processing the data from the entire duration of the earthquake's source. For large earthquakes such as the M 9.1 Tohoku earthquake off the coast of Japan, the source duration may be almost three minutes long. If the calculations for magnitude are performed before the entire source rupture is complete, the magnitude may be severely underestimated, as in the case of Tohoku, where initial calculations estimated an M 8.0 event, 32 times smaller than the true seismic moment. How could Early Warning Systems, such as those in Japan, be improved if we could know the final magnitude of an earthquake within just the first few seconds of rupture? The difference in timing with this type of improvement would only be seconds or minutes, but even that short time can be quite crucial. High speed trains, nuclear power plants, and other sensitive operations could be shut down prior to the arrival of destructive surface waves, which wreak irreparable damage.

In light of the possible significant improvements to the ability to cope with these colossal natural disasters, seismologists have been working for some time to understand the beginning rupture processes of large earthquakes. If large earthquakes do begin differently from small earthquakes, perhaps there is predictive information locked within that beginning signal. Though it was thought for many years that all earthquakes begin the same way, i.e., that they are self-similar, more seismologists are starting to recognize that large earthquakes have some unique characteristics in their initial P-wave signal.

Seismologist have found that examining the first few seconds of the P-wave arrival in the seismogram often reveals a weak, short duration signal, hereafter referred to as the seismic nucleation phase (SNP), before the full P-wave amplitude is observed [e.g., *Umeda*, 1990; *Ellsworth* and *Beroza,* 1995]. The SNP is thought to originate from a small area on the fault rupturing just prior to the full rupture, as shown in **Figure 1**. *Umeda* [1990] called the arrivals of these two P-wave signals P1 and P2, respectively. A report by *Ellsworth* and *Beroza* [1995] demonstrated that, in 30 earthquakes with moment magnitudes ($M_w$) ranging from 2.6 to 8.1, the duration and magnitude of the SNP were found to correlate with the magnitude of the earthquake. In other words, the longer the SNP (or P2-P1 time) and the greater the amplitude of the SNP signal, the greater the final magnitude of the earthquake. In contrast, a publication examining the SNP in the 1995 Ridgecrest, CA sequence by *Mori* and *Kanamori* [1996] found that the characteristics of the beginning of the P-wave are independent of the magnitude of the earthquake. In other words, *Mori* and *Kanamori* [1996] found the large and small earthquakes to be self-similar—that they have no discernible differences in their initial signal. The former

studies might indicate a predictive power in the beginning waveforms; the latter study would not.

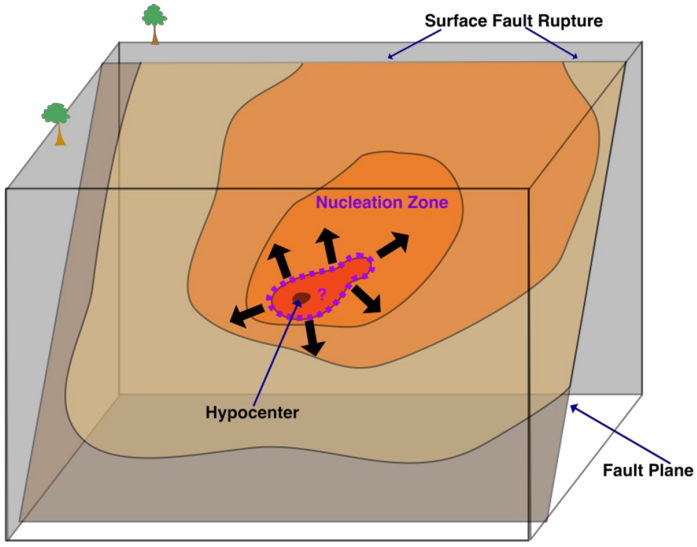


Figure 1: Visual representation of the nucleation zone on a fault plane. From there, the rupture propagates outward.

In order to truly examine the possibility of correlating the SNP with the total earthquake magnitude, we needed a more detailed analysis of a bigger catalogue of events than those previously studied. As such, we began our study by performing an analysis of large earthquakes to determine what relationship exists between the SNP and the earthquake magnitude. Since *Ellsworth* and *Beroza* [1995] found that the duration and amplitude of the SNP increase with the magnitude of the event, examining large earthquakes should make the SNP easier to detect because their SNPs will have a higher signal-to-noise ratio and longer duration than those of smaller earthquakes. In our study, we examined 68 events of M 7.5-8.0 to determine for which events the SNP is detectable, as well as to measure its duration. If the relationships of *Ellsworth* and *Beroza* [1995] are held, the

SNPs of these events shall have magnitudes larger than 6 and durations longer than 5 s, and therefore should be able to detect even using teleseismic data. The SNP is clearly detectable in 28 events, with 33 events showing no nucleation phase, two having too much noise or not enough stations to tell, and four with SNPs whose focal mechanisms are opposite from that of the main event. A detailed analysis was performed to evaluate the correlation between the occurrence of the SNP and certain aspects of the event. The aspects examined were: focal mechanism, hypocenter depth, geographic location (plate boundaries), and for thrust events: age of the crust, seafloor sediment thickness, and angle of the down-going slab.

The main questions we hoped to answer with this study were:

- What makes a particular earthquake exhibit a seismic nucleation phase?
- Are there causal relationships between the SNP and the hypocenter depth, focal mechanism, fault geometry and tectonic environment?

## II. Background

In order to understand large earthquakes, we must first understand how earthquakes begin. In particular, we must understand what makes large earthquakes different from small earthquakes. Are there clues during the initial rupture stages that tell us whether an earthquake will be small or large?

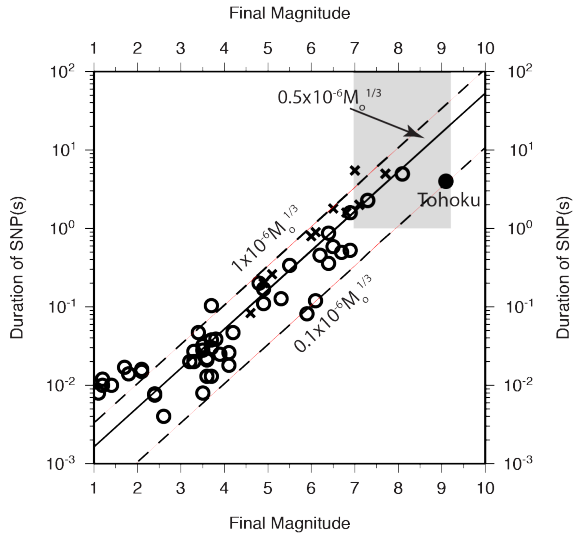


Figure 2: Comparison of durations of SNP with the final magnitudes. A scaling relationship of seismic moment $M_o$ versus the duration of the SNP, *v*. The straight line has a slope of 1/3, indicating a scaling of $M_o \sim v^{1/3}$. The crosses and open circles denote the events collected by Umeda [1990] and Beroza and Ellsworth [1996], respectively. The 2001 M 9.1 Tohoku earthquake is also plotted.

As far as we know, the first person to relate the duration of the SNP to the final earthquake magnitude was *Umeda* [1990]. Umeda's study was limited to large, shallow earthquakes. He examined 10 events in Japan from 1978-1987, from 0-80 km depth, and from magnitude 4.6-7.7. In his paper, Umeda stated that some large earthquakes have two stages of rupture. He also wrote that the time between the stages, P2-P1 (i.e., the duration of the SNP) is proportional to the earthquake magnitude (**Figure 2**.). The longer the preliminary rupture takes, the larger the secondary failures of the fault leading to a larger magnitude event. This relationship "strongly suggests that the two rupturing events corresponding to phases P1 and P2 do not occur at random but that they have a cause and effect relationship." [Umeda, 1990]. The paper explains in detail how the shear strain waves from the initial rupture phase are capable of triggering secondary ruptures.

The critical shear strain is defined as the strain that must be overcome for the fault to rupture. Of course, there exists some amount of pre-earthquake shear strain on the fault already. If the shear strain waves propagated by the initial rupture are greater than the

difference between the critical strain and the pre-earthquake shear strain, then the fault continues to rupture, leading to a large rupture area and large magnitude.

An important point made in the summary of Umeda's paper, has to do with the "trigger level" or the difference between the pre-earthquake shear strain and the critical shear strain in a medium. The critical shear strain of an area in the earth's crust is related to the rock or fault strength—basically, how much total shear strain is needed to cause a rupture. If the trigger level in a certain area is high, i.e., if the shear strain of the pre-earthquake stage is low and the critical shear strain is high, a longer P2-P1 (SNP) is needed to develop the secondary ruptures. In some fault zones, the difference between the pre-earthquake shear strain and the critical shear strain may be small. In this case, a shorter SNP could provide the necessary shear strain waves to overcome the critical shear strain and rupture a large area. So the relationship between SNP duration and the magnitude of the resulting earthquake may break down in areas with higher pre-earthquake shear strain or with low critical shear strain.

The next study to address the initial rupture phase of an earthquake and, in fact, to name this phase the Seismic Nucleation Phase (SNP), was by *Ellsworth* and *Beroza* [1995]. They conducted a survey of the initial P-wave observations in near-source records of 48 earthquakes, spanning a magnitude range of M 1.1 to 8.1. In their study, Ellsworth and Beroza found a definite correlation between the earthquake magnitude and both the duration and magnitude of the SNP. Specifically, they related the seismic moment, $M_o$, with the duration of the SNP, $v$, and found that $M_o$ is proportional to $v^3$ (**Figure 2**.) Like

the relationship found by Umeda, it is important to note that for a given *v* there is a range of associated magnitudes spanning two orders of moment magnitude. So using just this relationship, a magnitude could not be predicted with great precision.

To measure the duration of the SNP, *Ellsworth* and *Beroza* [1995] examined the beginning waveform of the velocity record. Marking the start and end of the SNP was done by visually examining these records. An example of some of these waveforms is shown in **Figure 3**.

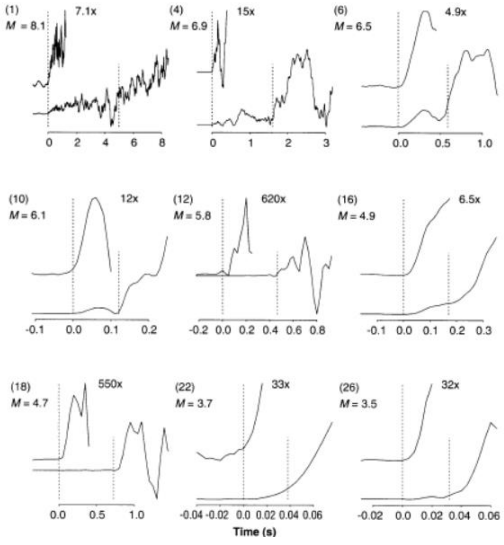


Figure 3: A figure from *Ellsworth* and *Beroza* [1995] shows a representative set of the velocity seismograms used in their analysis. Each seismogram is plotted at two amplitude scales with the higher magnification (top) showing the onset of the first P wave (SNP.) The interval between the first dashed line (zero) and the second dashed line spans the duration, *v*, of the SNP.

*Ellsworth* and *Beroza* [1995] also proposed two new models for the initial earthquake rupture process to explain the existence of this SNP. These models differ significantly from the previously accepted self-similar rupture model. They proposed two models named the "cascade" model and the "preslip" model. These, along with their

representative velocity records, are compared with the self-similar model in **Figure 4**. It should be noted that, though both the cascade and the preslip models would explain the presence of the SNP, only the preslip model would lead to the possibility of earthquake magnitude prediction based on the SNP.

Please merge Figure 4a, 4b, 4c in one text box!!!

Figure 4 a): Self-similar model for the earthquake nucleation process. In this model, no SNP is seen, just linear energy growth.

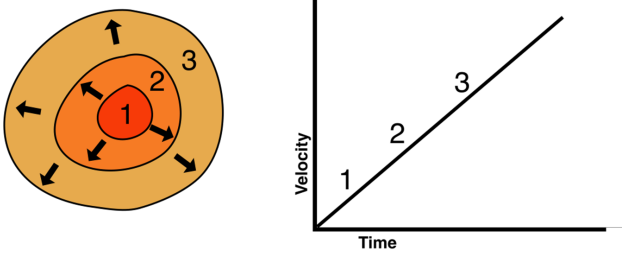


The cascade model describes an initial rupture that begins with slip in one small area that triggers slip in subsequent areas. The total magnitude of the earthquake is determined by how much area slips subsequently, not by the size or duration of the initial rupture (SNP).

Figure 4 b): Cascade model for earthquake nucleation process. In this model, a small patch ruptures, triggering successive small ruptures.

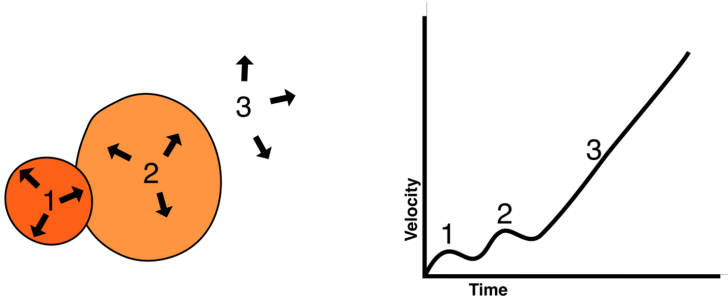

In contrast, the preslip model proposes that aseismic slip begins in the nucleation zone, followed by more violent slip of this zone (marked by the visible SNP), that triggers rupture of the whole fault area. In this model, both the SNP and the total earthquake are understood to be determined by the aseismic (pre) slip, this model explains why a relationship between the SNP duration and the total magnitude of the earthquake is possible.

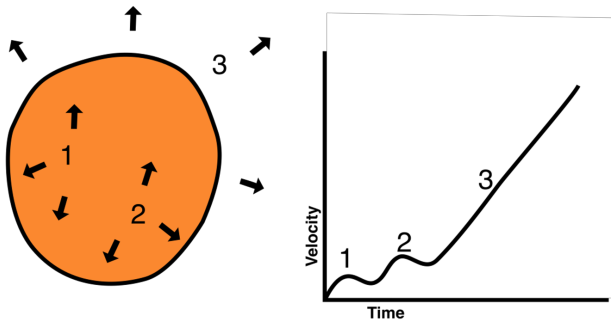


Figure 4 c): Preslip model for earthquake nucleation. This model proposes a period of aseismic slip prior to the small amounts of seismic slip marked by times 1 and 2.

An opposing study by *Mori* and *Kanamori* [1996] disputed the relationship between the SNP and the earthquake magnitude by examining the 1995 Ridgecrest, California sequence of earthquakes. These events had a magnitude range of M 1.5 to M 4.2 at hypocentral distances of 9 to 14 km recorded at a single station, as well as some smaller magnitude events from a more sensitive station in the area. They excluded events from their study only if the ambient noise obscured the beginning of the P wave arrival. The difficulty here is that, for such small magnitude events, even with a close station to record the waveforms, the SNP would be nearly impossible to detect above the ambient noise level. *Mori* and *Kanamori* [1996] also added that the signal from a slip over the small nucleation region on the fault would not be resolvable with the standard seismic

instrumentation deployed in California in 1995, at least not for events of magnitude less than 5.0. **Figure 5** shows their velocity seismograms for the Ridgecrest sequence on the left and, for comparison, synthetic seismograms for these events using the Sato and Hirasawa source [Sato and Hirasawa, 1973], taking into account the attenuation. In the observations, the observed initiations indeed have smaller slope but it could also be caused by the earth attenuation.

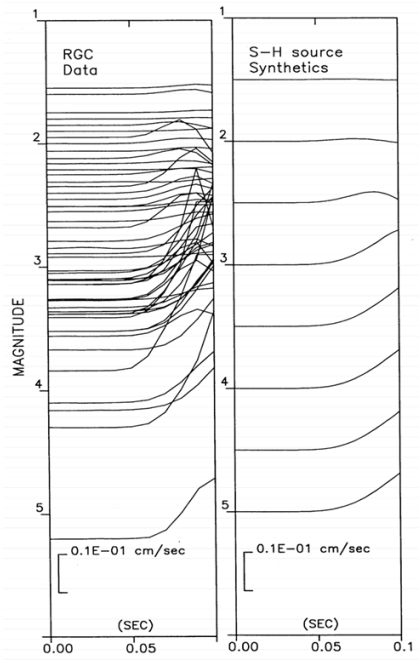


Figure 5: Left-hand graph shows the beginning of P waves recorded at station RGC from *Mori* and *Kanamori* [1996]. Magnitudes range from M 1.5 to M 4.2. The right-hand side of the figure shows synthetic seismograms calculated using a *Sato* and *Hirasawa* [1973] source convolved with an attenuation operator using t*=0.02 sec and the short-period instrument response.

In response to the *Mori* and *Kanamori* [1996] paper refuting the SNP relationship with final earthquake magnitude, *Beroza* and *Ellsworth* [1996] also examined the 1995 Ridgecrest, California sequence to determine the existence of a nucleation phase. They found that the smaller M ~2 events did not have detectable SNPs, but they conclude this may be because the expected SNP has a very short duration (<0.01 sec) and might not be observable in these data. But the larger M ~4 events do show a clear SNP. **Figure 6** shows the seismograms of the displacement records of the Ridgecrest sequence. A short,

~0.1-0.2s, weak phase is visible in the M3.8-M4.9 events. It can be seen that there are temporal variations in these earlier portions of waveforms, inconsistent with the smoothing effect of earth attenuation.

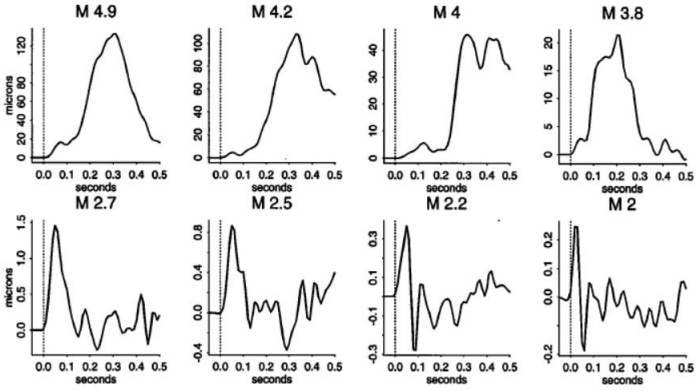


Figure 6: Displacement seismograms for earthquakes recorded at the digital accelerometer station RC1 for the 1995 Ridgecrest, California earthquake sequence, from *Ellsworth* and *Beroza* [1996]. The dashed vertical lines mark the P wave arrivals. The SNP is clearly visible in the larger (top row) events, but cannot be resolved, if present, in the smaller events (bottom row).

Although *Beroza* and *Ellsworth* [1996] did not find a relationship between SNP duration and earthquake magnitude in the Ridgecrest sequence, it's important to remember that this study only examined relatively small (< M 5.0) events. For these events, the SNP is understandably much shorter and with smaller amplitude. But it may also be that the relationship between SNP and earthquake magnitude does not hold true for small earthquakes.

Three known biases are associated with these previous studies in terms of data examined and distributions of earthquakes. First, because the duration and magnitude of the SNP in smaller magnitude events make the SNP difficult to distinguish from the ambient noise,

[*Ellsworth and Beroza,* 1995], the range of magnitudes of the events examined in both of the afore-mentioned studies is insufficient to make definitive statements about the nucleation phase of earthquakes with larger magnitudes. Second, the station coverage of these events is less than complete. Especially in the case of the Ridgecrest sequence, one or two stations were used to measure the events. Finally, most of these events occurred in California and Japan. It is not clear yet whether the relations derived from them can be used globally.

Motivated by these issues we analyze a group of 69 Mw 7.5-8.0 earthquakes occurring from 1994 to 2010 using the teleseismic data recorded by global seismic network. We find that only half of these earthquakes have detectable SNP. In the second part of this thesis we try to understand whether we can explain such an observations. We needed a better understanding of why some subduction zones show no SNP in one area and visible SNP in another area. As such, another paper was studied to give motivation for more analysis. *Ruff* [1989] explains two models for subduction zones where sediments from the seafloor are being dragged into the subduction zone by the subducting plate. *Ruff [1989]* points out that the two factors normally thought to control seismicity in subduction zones (rate of subduction and age of the subducting plate, see **Figure 7**) cannot always explain the occurrence of large earthquakes in some regions and creep in others. So *Ruff* [1989] set out to explain the exceptions by studying the seafloor sediments being subducted (and often accreted) by the subducting plate.

Figure 7: From *Ruff*, 1989, this graph shows the relationship between subduction zone characteristics and the size of the earthquakes in those zones. Older plates subducting slowly tend to have smaller earthquakes. Great earthquakes (M > 8.0) occur in zones where younger plates are subducting more quickly.

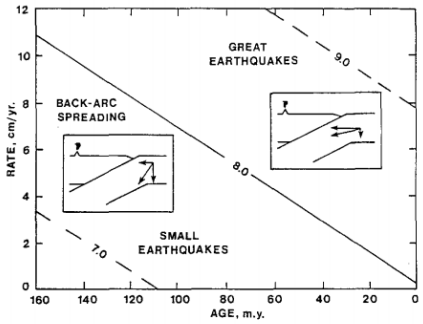


*Ruff* [1989] built upon a study by *Hilde* [1983], which had classified many of the world's subduction zones. *Ruff* [1989] chose to simplify the problem and use a binary classification: i) zones with excess trench sediments (ETS) and ii) zones with a horst and graben structure (HGS). The depth of the grabens is typically < 1 km, and the horizontal dimension is approximately 10 km. A well-developed horst and graben structure provides "buckets" which can erode the upper-plate and carry down sediments. **Figure 8** is a diagram from *Ruff* [1989], showing the two types of sediment subduction. The idea behind these models and how they affect seismicity is that the ETS would subduct coherent layers of sediments, leading to a smooth strength distribution. The HGS conversely, would have a heterogeneous strength distribution, where the contact between the plates alters between basaltic crust and chaotic sediments.

Figure 8: From *Ruff*, 1989, two models for the subduction of seafloor sediments. The horst and graben structure (HGS) model carries sediments in "buckets" whereas the excess trench sediments (ETS) subduct sediments smoothly.

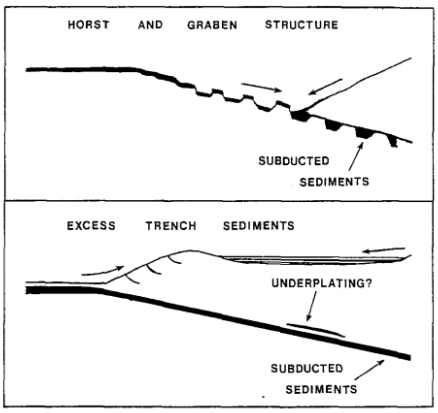


*Ruff* [1989] uses his study to explain why large (M > 8.0) earthquakes occur in some subduction zones and not in others. He finds that the majority of the largest interplate subduction zone earthquakes occur in ETS zones (**Figure 13**). We were intrigued by this idea and wondered how subducting sediments might affect the occurrence or the ability to detect the SNP in large earthquakes. We will discuss that idea as well as other "properties" of subduction zones.

## III. Data

Our study encompassed every M 7.5 to 8.0 earthquake from 1994 to 2010 worldwide, resulting in 68 events in total. By studying these high magnitude events, we gave ourselves the greatest possibility of detecting the SNP, as this phase is understood to be greater in amplitude and longer in duration than in smaller magnitude events [*Ellsworth* and *Beroza*, 1995].

We used broadband teleseismic data up to 8 Hz (low-pass filtered) from all global teleseismic stations (30 degrees to 90 degrees away from the source) that recorded the events. The advantage of teleseismic waves for this kind of analysis is two-fold. First, these waveforms have the greatest amount of station coverage, usually producing records from hundreds of stations. Teleseismic waves also have the majority of their travel path in the Earth's mantle, reducing signal frequency degradation by the Earth's crust. The disadvantage to teleseismic waves is their long travel path. By definition, teleseismic waves are recorded by stations that are at least 30 degrees away from the source. We further restricted the stations to be less than 90 degrees from the source, allowing them to travel a short (almost vertical) path through the Earth's crust but to not bounce off of the Earth's core (**Figure 9**.) Because of the amplitude degradation due to the long travel path, we stacked the signals to increase the signal-to-noise ratio. By design (choosing events from 1994 and later, when global station coverage became more extensive) we had a sufficient number of stations that recorded the events to allow stacking.

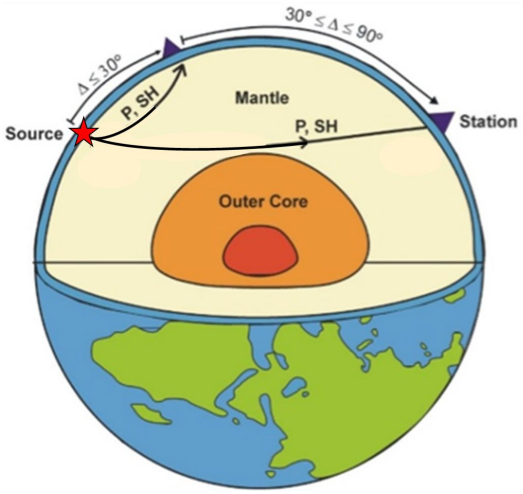


Figure 9: Teleseismic waves traveling from the source of an earthquake to the receiving station. Figure adapted from *Fielding et al*., 2011.

Data from the Global Seismic Network (GSN) were downloaded from the Incorporated Research Institutions for Seismology (IRIS) database. Data from the Virtual European

Seismic Broadband Network (VESBN) were downloaded from the Observatories and Research Facilities for European Seismology (ORFEUS) Data Center (ODC.) The map in **Figure 10** shows the geographical distribution of the events studied, along with our results regarding the visibility of the SNP in those events.

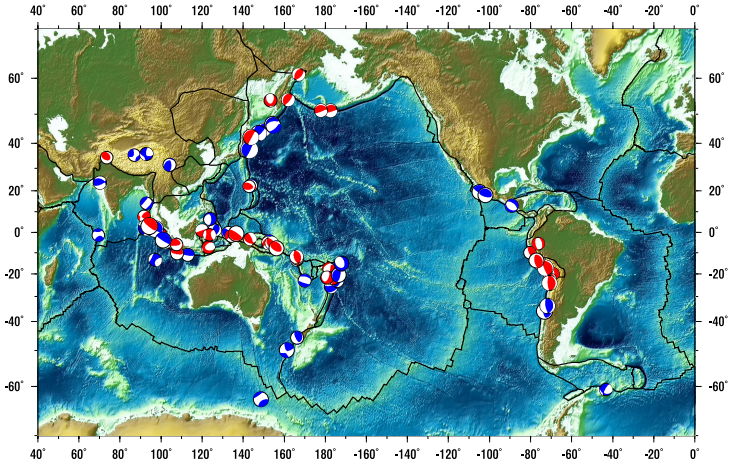

Figure 10: Locations of all events from this study as well as the M > 8.0 events from [*Ji*, 2011] are shown with beach balls representing their focal mechanisms. Blue beach balls denote events with visible SNP and red have no visible SNP. The larger beach balls are the M > 8.0 events.

National Oceanic and Atmospheric Administration (NOAA) freely distributes the global marine sediment thickness dataset through its National Geophysical Data Center (NGDC) [**Figure 11**]. These data were gridded in a spacing of 5 arc-minutes by 5 arc-minutes. The

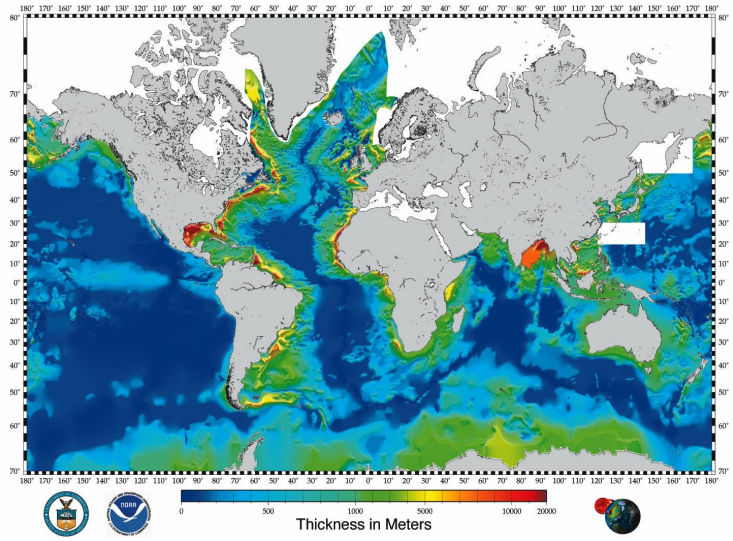


Figure 11: Taken from the NOAA website, this map shows the thickness in meters of the world's seafloor sediments.

sediment-thickness data were compiled mainly from the following three sources: 1) isopach maps that were previously published, including those from Ludwig and Houtz [1979], Matthias et al. [1988], Divins and Rabinowitz [1990], Hayes and LaBrecque [1991], and Divins [2003]; 2) results from ocean drilling from both the Ocean Drilling Program (ODP) and the Deep Sea Drilling Project (DSDP); 3) archived seismic reflection profiles at NGDC, and seismic data and isopach maps found in the United Nations' Intergovernmental Oceanographic Commission (IOC)'s International Geological-Geophysical Atlas of the Pacific Ocean [Udinstev, 2003]. To find the sediment thickness on the subducting plate, a line from the epicenter of the event, perpendicular to the trench, and onto the subducting plate was drawn in Google Earth; a data point was extracted from the gridded data every 10 km along this line. Then the data were graphed and the thicknesses for ~30 km preceding the trench on the subducting plate were averaged to give a single datum for the event. An example of this procedure is shown in **Figure 12**. As it can be seen in **Figure 11**, some areas did not have data coverage. Of the 42 thrust events examined, six had no seafloor sediment thickness data.

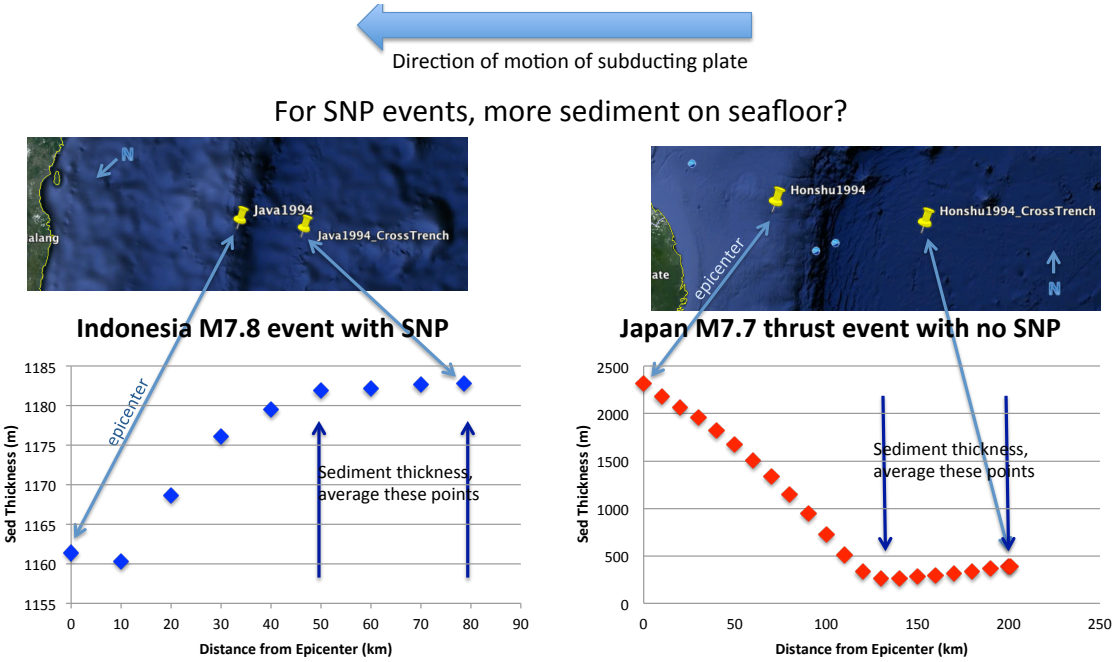


Figure 12: To get a single sediment thickness datum for each event, the thickness data for a line running perpendicular to the trench was extracted from the grid file and plotted. Then the points on the subducting plate preceding the trench are averaged.

To study the correlation between the thrust earthquakes with SNP and the age of the lithosphere of the subducting plate in thrust earthquakes, we used another dataset from the NGDC [**Figure 13**]. These data are gridded with two-minute resolution and are interpolated linearly in the direction of spreading between the oldest identified magnetic anomalies and geologic estimates of passive continental margin sediments [*Müller et al*, 2008]. To find the corresponding age for a given earthquake, a similar method was used as in the sediment thickness study.

Figure 13: A map from NOAA showing the age of the oceanic lithosphere.

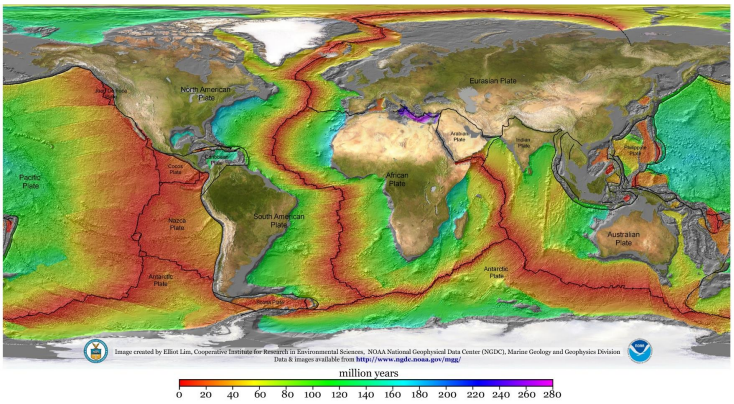


The data used to study the correlation between the earthquakes with SNPs and the angle of the subducting slab in thrust events was gathered from the Slab 1.0 model, provided by the United States Geographic Survey (USGS) website (URL). These data can be accessed by simply entering a latitude longitude combination into the website portal and recording the provided slab angle. This model was compiled by *Hayes et al.* [2012] using earthquake source locations and focal mechanisms.

Figure 14: A map from NOAA showing the age of the oceanic lithosphere.

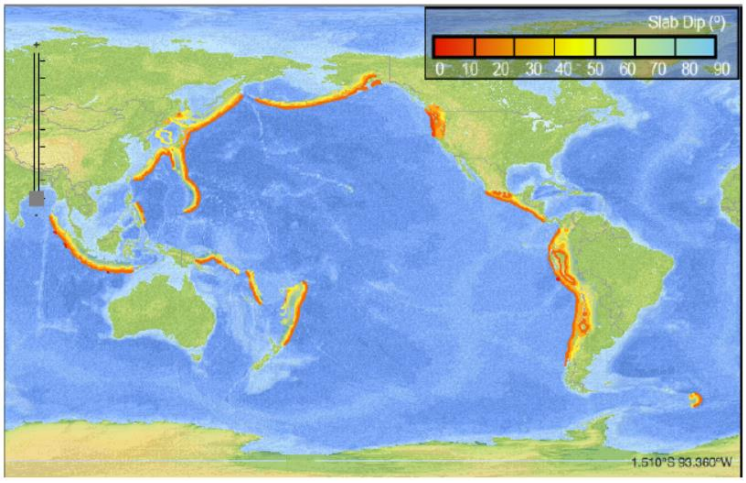

## IV. Methodology

This project went beyond previous examinations of SNP by including a greater number of earthquakes (69), globally distributed (no geographical bias), and with larger magnitude (7.5-8.0). Because previous research has shown that the duration and amplitude of the nucleation phase become smaller as the magnitude decreases [*Ellsworth* and *Beroza*, 1995], we expected that the events with high magnitudes will allow the best chance for detecting the SNP. Because our data included events from all over the world, we were able to examine characteristics of many types of earthquakes and earthquake zones.

Raw data (mini-seed files) were downloaded from the IRIS and ODC databases. We used Ji's code [*Ji*, 2011] to analyze the waveforms for a 90% correlation or better within a time window ranging from five seconds before and 10 seconds after the calculated first P-wave arrival; this window included the nucleation phase as well as the following phase, called the breakaway phase.

We include the breakaway phase since we can assume, for the purpose of these discussions, that the stations with similar breakaway waveforms also have similar seismic-nucleation phase waveforms, (*Ji*, 2011). Because the noise in the teleseismic

$$stack_N(t) = \sum_{k=1}^{K} \frac{W_{Nk} a_{Nk} u_k(t - \tau_{Nk})}{\sum_{k=1}^{K} W_{Nk}}, \quad \& \quad W_{Nk} = \frac{1}{a_{Nk}\sigma_k}$$

Figure 15: Here, stack(t) denotes the stacking waveform using the N-th record as the reference. Sigma k represents the standard deviation of noise estimated using the k-th friendly record on a window 5 seconds before the start of the P wave and 15 seconds in duration.

data comes mostly from ocean waves, and since we use stations at varying distances from the coast, the noise of these waveforms can be greatly reduced by stacking the signals according to the formula [*Ji*, 2011] shown in **Figure 15**.

By examining the seismograms from these correlated stations and the stacked waves, we were able to see which earthquakes exhibit an "obvious nucleation phase." An obvious nucleation phase was defined, as in the previous studies, by subjective visual interpretation as seen in **Figure 16**. After careful examination of these waves, we marked the beginning and ending times of these nucleation phases and note also the differing depths, directions of slip, and magnitudes of the total events, compared to the existence of a seismic nucleation phase (see **Table 1**.)

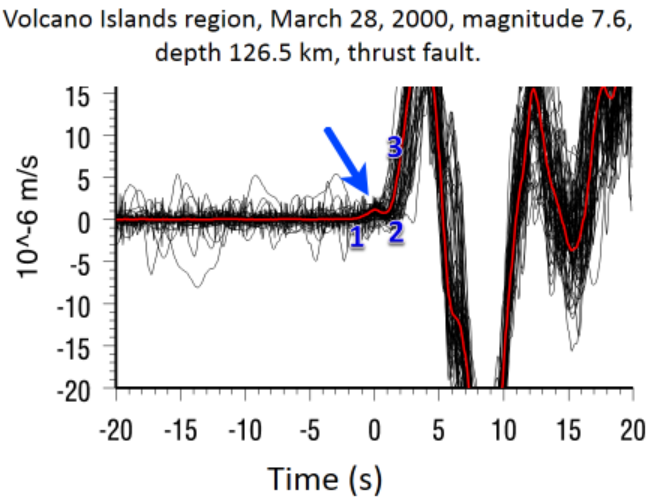


Figure 16: Here, we show an example of an event with a clear SNP, only visible after stacking the signals from the many global stations that recorded the event. The number 1 marks the beginning of the SNP. The number 2 marks the end of the SNP and the beginning of the breakaway phase. The number 3 marks the breakaway phase.

## Table 1 a)

Table of all events, 1994-2002

| Event Name | Date (YYMMDDHHMMSS) | Mw | Depth (m) | Nucleation Time (s) | Focal | Sediment Thickness (m) | Slab Angle (degrees) | Age of Plate (m.y.) |
|---|---|---|---|---|---|---|---|---|
| Fiji1994 | 199403092328 | 7.6 | 563 | NONE | normal | | 29 | |
| Java1994 | 199406021817 | 7.8 | 18 | 10.3 | thrust | 1182 | 5 | 126 |
| Honshu1994 | 199412281219 | 7.8 | 27 | NONE | thrust | 274 | 13 | 130 |
| Loyalty1995 | 199505162012 | 7.7 | 20 | 3.6 | normal | | | |
| Chile1995 | 199507300511 | 8 | 46 | NONE | thrust | 110 | 22 | 55 |
| Solomon1995 | 199508161027 | 7.7 | 30 | NONE | thrust | 458 | 28 | 35 |
| Jalisco1995 | 199510091535 | 8 | 33 | 1.6 | thrust | 13 | 33 | 15 |
| Kurile1995 | 199512031801 | 7.9 | 33 | 2.5 | thrust | 479 | 24 | 115 |
| Minahassa1996 | 199601010805 | 7.9 | 24 | NONE | thrust | 1697 | | 35 |
| Peru1996 | 199602211251 | 7.5 | 10 | NONE | thrust | 163 | 12 | 35 |
| Aleutian1996 | 199606100403 | 7.9 | 33 | NONE | thrust | 210 | | 55 |
| Flores1996 | 199606171122 | 7.9 | 587 | NONE | normal | | | |
| Peru1996 | 199611121659 | 7.7 | 33 | NONE | thrust | 316 | 15 | 45 |
| SantaCruz1997 | 199704211202 | 7.7 | 33 | NONE | thrust | 109 | 56 | 5 |
| SoFiji1997 | 199710140953 | 7.8 | 167 | NONE | normal | | 55 | |
| Tibet1997 | 199711081002 | 7.5 | 33 | 6.73 | strike-slip | | | |
| Kamchatka1997 | 199712051126 | 7.8 | 33 | NONE | thrust | | 20 | 99 |
| CeramSea1998 | 199811291410 | 7.7 | 33 | 11.8 | strike-slip | | | |
| Turkey1999 | 199908170001 | 7.6 | 17 | 1.9 | strike-slip | | | |
| Taiwan1999 | 199909201747 | 7.7 | 33 | 3.5 | thrust | | | 51 |
| VolcanoIsland2000 | 200003281100 | 7.6 | 127 | 3.5 | normal | | 50 | |
| Sulawesi2000 | 200005040421 | 7.6 | 26 | NONE | strike-slip | | | |
| Sumatra2000 | 200006041628 | 7.9 | 33 | 4.9 | strike-slip | | 18 | |
| Solandian2000 | 200006181444 | 7.9 | 10 | 1.6 | strike-slip | | | |
| NewIrelandB2000 | 200011160454 | 7.8 | 30 | 4.8 | strike-slip | | 29 | |
| NewIrelandC2000 | 200011160742 | 8 | 33 | too NOISY | thrust | | 66 | |
| NewBritain2000 | 200011172101 | 7.8 | 33 | NONE | thrust | 379 | 29 | 55 |
| CentralAm2001 | 200101131733 | 7.7 | 60 | 1.8 | normal | | 42 | |
| India2001 | 200101260316 | 7.7 | 16 | ~1 | thrust | | | |
| CoastPeru2001 | 200107070938 | 7.6 | 33 | 5.6 | thrust | 113 | 18 | 55 |
| Xinjiang2001 | 200111140926 | 7.8 | 10 | 3.6 | strike-slip | | | |
| Philippine2002 | 200203052116 | 7.5 | 31 | 3.0 | thrust | 767 | | 43 |
| Fiji2002 | 200208191101 | 7.7 | 675 | NONE | normal | | 28 | |
| SouthFiji2002 | 200208191108 | 7.7 | 580 | too NOISY | thrust | | 44 | |
| NewGuinea2002 | 200209081844 | 7.6 | 13 | NONE | thrust | 599 | | |
| Indonesia2002 | 200210101050 | 7.6 | 10 | NONE | strike-slip | | | |
| Alaska2002 | 200211032212 | 7.9 | 5 | NONE, began with thrust | strike-slip | | | |

Table 1 b)

Table of all events, 2003-2010

| Event Name | Date (YYMMDDHHMMSS) | Mw | Depth (m) | Nucleation Time (s) | Focal | Sediment Thickness (m) | Slab Angle (degrees) | Age of Plate (m.y.) |
|---|---|---|---|---|---|---|---|---|
| Jalisco2003 | 200301220206 | 7.6 | 24 | 6.5 | thrust | 394 | 25 | 5 |
| Carlsberg2003 | 200307152027 | 7.6 | 10 | 7.3 | strike-slip | | NaN | |
| ScotiaSea2003 | 200308040437 | 7.6 | 10 | 3.0 | strike-slip | | NaN | |
| Aleutian2003 | 200311170643 | 7.8 | 33 | NONE | thrust | 387 | NaN | 53 |
| Timor2004 | 200411112126 | 7.5 | 10 | 3.3, reverse polarity | thrust | 1346 | NaN | |
| Chile2005 | 200506132244 | 7.8 | 116 | NONE | normal | | 23 | |
| NewIreland2005 | 200509090726 | 7.6 | 90 | NONE | thrust | | 60 | 138 |
| Peru2005 | 200509260155 | 7.5 | 115 | NONE | normal | | 2 | |
| Pakistan2005 | 200510080350 | 7.6 | 26 | NONE | thrust | NaN | NaN | |
| BandaSea2006 | 200601271658 | 7.6 | 397 | 0.93 | strike-slip | | NaN | |
| Siberia2006 | 200604202325 | 7.6 | 22 | NONE | thrust | NaN | NaN | |
| Tonga2006 | 200605031527 | 8 | 55 | 5.1 | thrust | 29 | 25 | 5 |
| Indonesia2006 | 200607170819 | 7.7 | 20 | NONE | thrust | 709 | 7 | 107 |
| MoluccaSea2007 | 200701211127 | 7.5 | 22 | 2.8 | thrust | 1020 | NaN | |
| Jawa2007 | 200708081704 | 7.5 | 280 | NONE | thrust | 700 | 64 | 103 |
| Peru2007 | 200708152340 | 8 | 39 | NONE | thrust | 200 | 18 | 45 |
| Sumatra2007 | 200709122348 | 7.9 | 35 | NONE | thrust | 639 | 21 | 68 |
| VolcanoIslands2007 | 200709281338 | 7.5 | 260 | NONE | thrust | 130 | 62 | 140 |
| Chile2007 | 200711141540 | 7.7 | 40 | NONE | | 104 | 24 | NaN |
| Fiji2007 | 200712090728 | 7.8 | 153 | 5.9 | thrust | 111 | 59 | NaN |
| China2008 | 200805120628 | 7.9 | 19 | 2.9 | thrust | NaN | NaN | |
| Sea_of_Okhotsk2008 | 200807050212 | 7.7 | 633 | NONE | normal | | 63 | |
| Indonesia2009 | 200901031943 | 7.7 | 17 | 12.5 | thrust | 798 | NaN | 1 |
| Tonga2009 | 200903191817 | 7.6 | 31 | 2.0 | thrust | 41 | 8 | 55 |
| NewZealand2009 | 200907150922 | 7.8 | 12 | 5.5 | strike-slip | | NaN | |
| India2009 | 200908101955 | 7.5 | 24 | 1.6 | normal | | NaN | |
| Sumatra2009 | 200909301016 | 7.6 | 81 | NONE | thrust | 907 | 32 | 55 |
| VanuatuIslands2009 | 200910072203 | 7.7 | 35 | NONE | thrust | 36 | 36 | 5 |
| SantaCruzIslands2009 | 200910072218 | 7.8 | 45 | NONE | thrust | 38 | 47 | 5 |
| Sumatra2010 | 201004062215 | 7.8 | 31 | 3.0 | thrust | 1198 | 20 | 46 |
| India2010 | 201006121926 | 7.5 | 35 | NONE | thrust | 615 | NaN | 67 |
| Philippines2010 | 201007232251 | 7.6 | 578 | 5.8 | normal | | NaN | |

One caveat of this method is related to the focal mechanism of each earthquake, and whether the stations that we use for stacking are located near a nodal plane of the earthquake. If this were the case, the nucleation phase arrival would be distorted by the stacking process, because it would manifest quite differently across nodal planes. To address this potential problem, we plotted the focal mechanism along with the station locations to see how the nodal planes correlated with stations and deliberately chose stations prior to the stacking process to ensure proper distribution. In this study, we projected the station locations onto a focal sphere inferred from the Global Centroid Moment Tensor (GCMT, http://www.globalcmt.org) (**Figure 17).**. During this time we also tried using slightly longer and shorter time windows for the correlation among stations for each event. The first stage of the analysis used a 15-second window: five seconds before and ten seconds after the picked P-wave. The picked P-wave was part of the event data from IRIS and ODC. Three events were changed (lost the signal of the

SNP) by rerunning the stacking with more carefully chosen stations. No events had significant changes from trying different time windows.

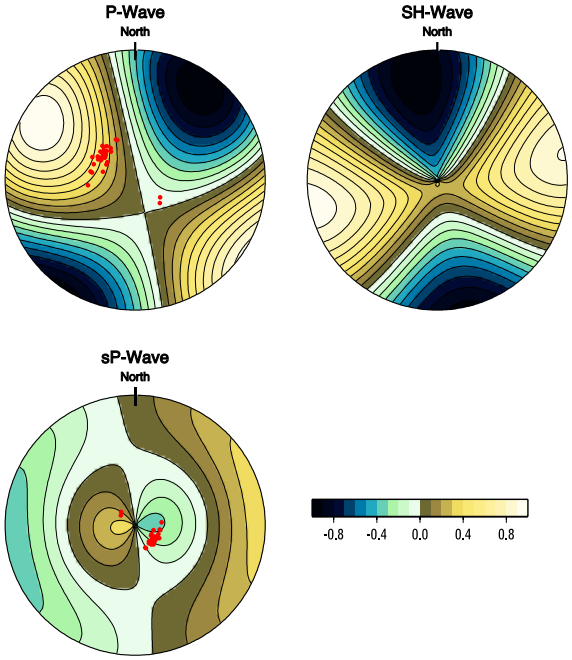


Figure 17: This figure shows the stations used for stacking are shown plotted on the projected focal mechanism of a shallow strike-slip earthquake, M 7.5, in Tibet in 1997. No clustering at the nodal plane is observed for this event.

We found that strike-slip events were much more likely to exhibit a nucleation phase than other focal mechanisms. Thrust and normal events were almost evenly distributed between clear SNP and no SNP (**Figure 18 b**.)

About sixty percent of earthquakes we studied are thrust earthquakes in subduction zones. In the case of the subduction zones, some geographical patterns were noticed that sparked further interest in these events. Certain areas along subduction zones had clusters of SNP-visible events; it was thought that these patterns might correlate with physical aspects of the subducting plate. We gathered information about the seafloor sediment thickness, age of the subducting plate, and angle of subduction for all thrust events.

Unfortunately there were no globally consistent correlations between SNP and seafloor sediment thickness, age of the subducting plate, or angle of the down-going slab.

## V. Results

The normalized and stacked teleseismic records of 68 global earthquakes of magnitude (M) 7.5-8.0 were examined for existence of the seismic nucleation phase (SNP). Of the 68, 28 events in total showed a clear SNP, 35 showed no visible SNP, two events were too noisy to tell, and four events had a reverse-polarity SNP. (**Figure 18 a**). As the GCMT solution represents the average focal mechanism of an earthquake, an event with reverse-polarity SNP suggests that its initiation stage has a different focal mechanism. The total number of events with SNP is 32, 47.7% of the earthquakes with good signal-to-noise ratios. The frequency of Mw>7.5 events with detectable SNP is correlated with its source depth. As shown in Figure 18b, For earthquakes with hypocenter depth <200km, about half exhibited visible SNP, while for earthquakes deeper than 200 km, only one of nine had a visible SNP (**Figure 18 b**). The frequency of an Mw>7.5 event with detectable SNP also depends on focal mechanism. Nine out of the 12 strike-slip events (75%) have detectable SNPs, while for thrust and normal fault earthquakes, there were fewer than half of the events with a visible SNP (**Figure 18 c**).

Figure 18 a): All events shown with visible SNP, No SNP, Noisy and Reverse focal events.

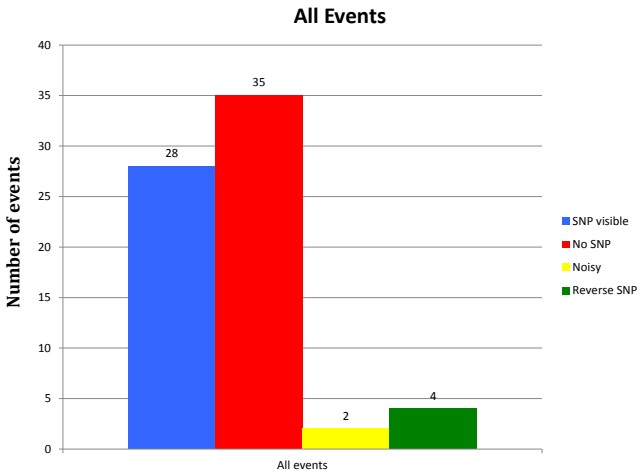


Figure 18 b): Events shown categorized by hypocenter depth.

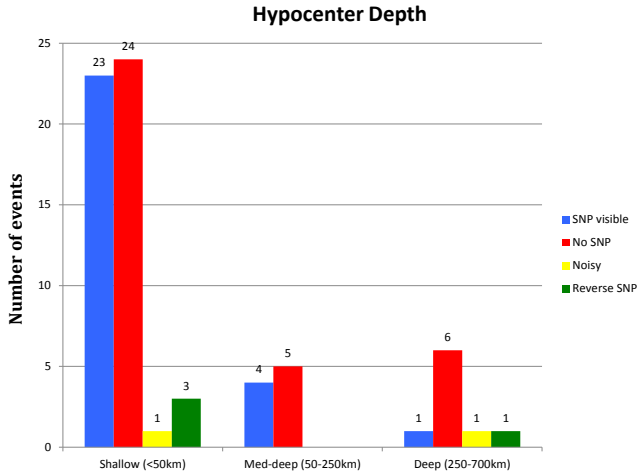

Figure 18 c): Events shown categorized by focal mechanism. Notice that strike-slip events tend to show SNP.

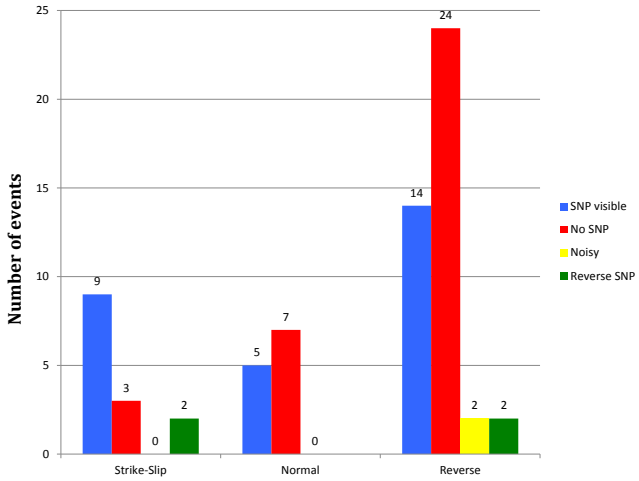


We also found that, in events with detectable SNPs, the durations fall within the expected range using the relationship previously established by *Ellsworth* and *Beroza* [1995], as shown in **Figure 19**.

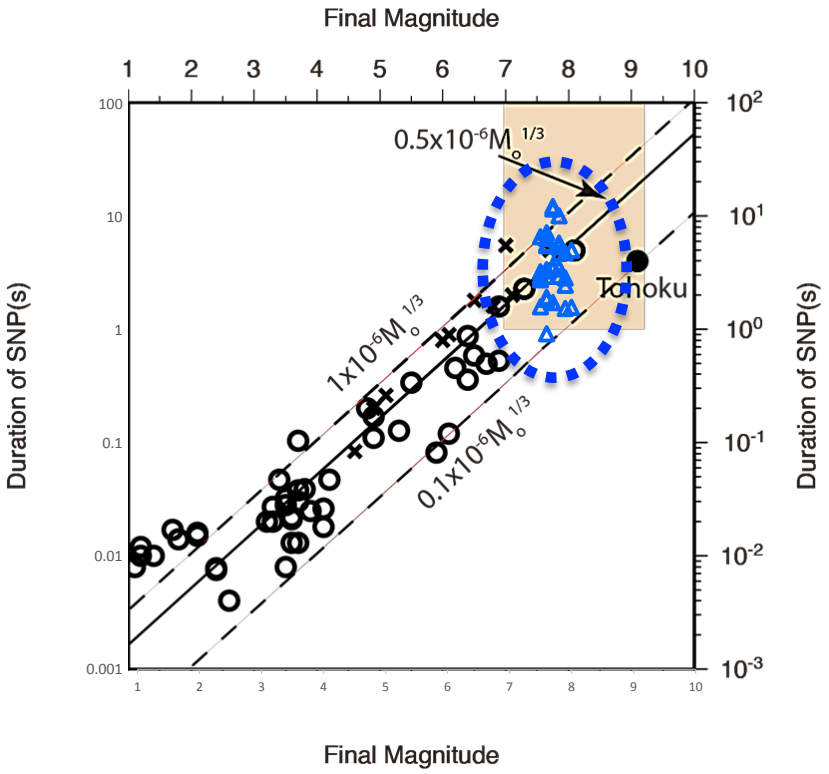


Figure 19: Here are the events shown in Figure 1 along with the events from this study. The durations of the SNPs measured in this study fall within the expected range.

About 60% earthquakes in our category are thrust events along the subduction zones, in which only 40% have detectable SNPs. In trying to determine what properties of subduction zones might influence the occurrence or ability to detect the SNP in thrust earthquakes, we found the following.

## Seafloor Sediment Thickness:

Inspired by the work of *Ruff* [1989], we investigated whether there is a correlation between the seafloor sediment thickness on the subducting plate of thrust earthquakes and the events with SNP.

Figure 20: A zoomed in view of the Nazca-South American subduction zone. On the left is a map from this study of M 7.5-8.0 events and the [*Ji*, 2011] study of M >8.0 events. The blue beach balls indicate a clear SNP and the red beach balls indicate no clear SNP. On the right is the seafloor sediment thickness map from NOAA. There seems to be a correlation in this subduction zone between the SNP and thicker seafloor sediments.

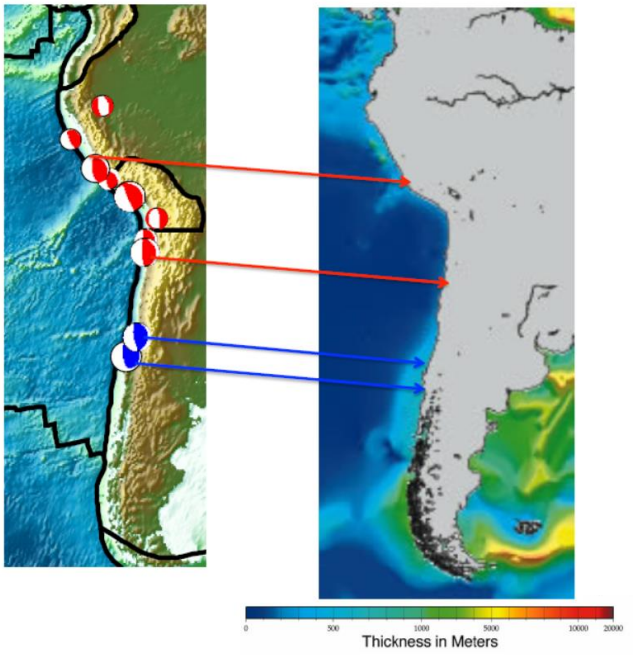


**Figure 20** compares the Mw>7.5 events and the marine sediment thickness along the Nazca-South American subduction zone. As it can be seen, the majority of the events did not have a detectable SNP. The events with no SNPs are clustered around the northern section of the subduction zone. The two events with detectable SNPs are located in the southern portion of the subduction zone. As can be seen in the map on the right of **Figure**

Figure 21: A histogram showing the distribution of events with SNP and the seafloor sediment thickness.

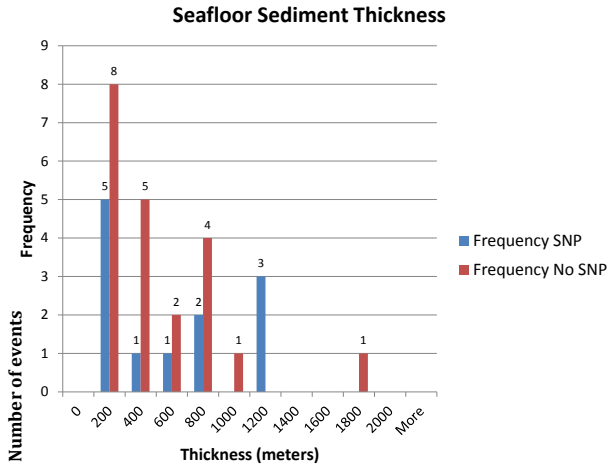

**20**, the thickness of the near-trench sediment is also bi-distributed, being thinner to the north and thicker to the south. The events without SNP correlate with the subduction zone without thick near-trench sediments. So we see in this study, the existence/visibility of the SNP correlates very well with the thickness of the sediment on the seafloor, in this particular subduction zone. When we expand the study to include all subduction zone events, the correlation seems to disappear. We found that the hypocenters of all the earthquakes in this catalog are found within the regions with near-trench sediment thickness less than 2000 m. In fact, 32 of 33 events are in zones with sediment thickness less than 1200 m. We noticed a clear trend that the number of such large earthquakes decreases with the sediment thickness. **Figure 21** shows the histograms of earthquakes in different ranges of sediment thickness. Here, no strong pattern is observed. There appears to be equal distribution of events with and without SNP across all thicknesses. So we tried plotting the seafloor sediment thickness with the hypocenter depth of the earthquake to see if a pattern emerged. **Figure 22 a) and b)** shows the cross-section of sediment thickness with hypocenter depths. As expected, most large earthquakes nucleated at depths shallower than 50 km. Note that for these shallow earthquakes, there is no clear correlation between SNP events and sediment thickness, but most events with no SNP are correlated with sediment thickness less than 700 m. This leaves a cluster of five events with observable SNP in the regions associated with 700-1200 m of sediments without any No SNP events. It seems that shallow earthquakes with thick seafloor sediments tend to exhibit an SNP. For deeper earthquakes, such a correlation cannot be seen.

Because this pattern of shallow, thick sediment events with SNP was observed, we decided to also run this analysis on events from the *Ji* [2011] study of the SNP of M >8.0 events. When these events were added to the study on sediment thickness, the pattern was confirmed that events with no SNP seem to occur in subduction zones with thin (< 700 m) sediment on the seafloor of the subducting plate, while events with SNP occur at every level of sediment thickness.

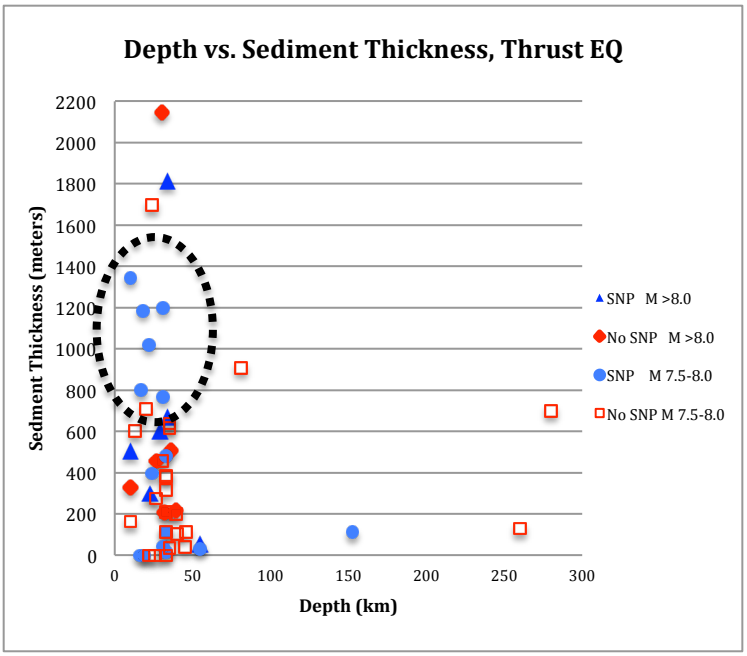


Figure 22 a): A cross plot of depth vs. sediment thickness for events M 7.5-8.0 from this study as well as the M >8.0 events from [Ji, 2011]. Notice the pattern of shallow, thick sediment events with SNP.

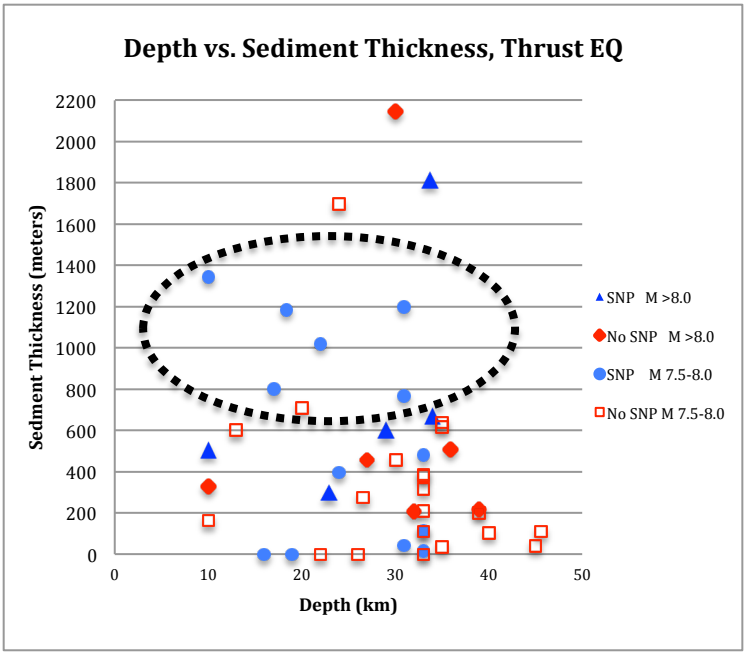


Figure 22 b): A zoomed-in cross plot of depth vs. sediment thickness for events M 7.5-8.0 from this study as well as the M >8.0 events from [Ji, 2011]. Notice the pattern of shallow, thick sediment events with SNP. The horizontal axis of this plot has been limited to examine the shallow events.

## Age of the Oceanic Lithosphere:

The maps in **Figure 23** shows the pattern along the Nazca-South American subduction zone [*Müller et al*, 2008]. When compared with the age-of-the-seafloor map, the pattern seems to indicate that the events with SNP occur in younger crust than the events with no SNP. When events from all subduction zones are considered, however, the pattern becomes unclear. We found that all study events occurred in subduction zones where the age of the subducting plate was between 10 and 150 ma. But there is no correlation seen between the age of the subducting plate and SNP. The graph in **Figure 24** shows the histogram of the examination of the age of the lithosphere of subducting plates of thrust events. The graph in **Figure 25** shows a cross-section of the hypocenter depth with the age of the lithosphere. There does not seem to be a clustering of events indicating a correlation between SNP and age of the subducting plate with the hypocenter depth.

Figure 23: A zoomed-in view of the Nazca-South American subduction zone. On the left is a map from this study of M 7.5-8.0 events and the [*Ji*, 2011] study of M >8.0 events. The blue beach balls indicate a clear SNP and the red beach balls indicate no clear SNP. On the right is a map from NOAA showing the age of the lithosphere of the subducting plate.

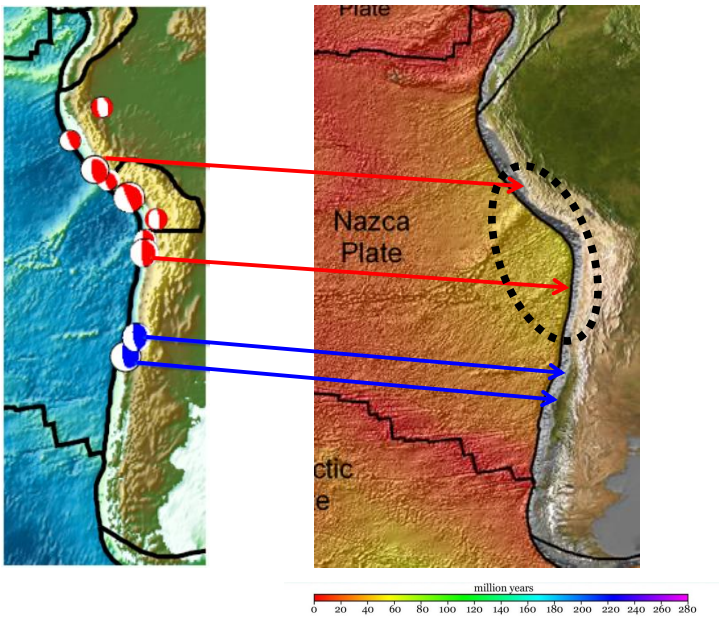

Figure 24: A histogram showing the results from the age-of-the-subducting-plate study. No pattern is seen here.

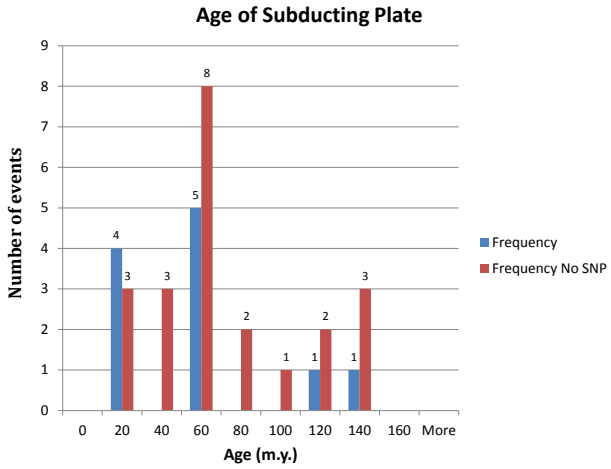


Figure 25: A cross plot of depth vs. the age of the lithosphere of the subducting plate. No pattern is seen here.

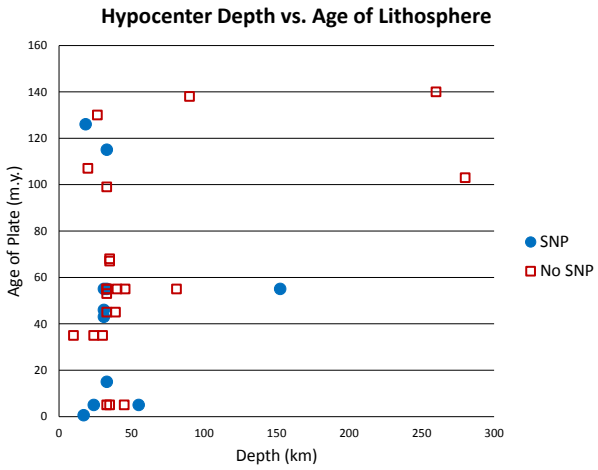


## Angle of the Subducting Plate:

**Figure 26** shows a map of the events along the Nazca-South American subduction zone compared with a map of the angle of the subducting plate from the USGS Slab 1.0 model. [*Hayes et al*, 2012] We found that the subduction zone events in this study occurred in

zones where the subduction angle was between five and 75 degrees. There is no correlation seen between SNP and angle of the subducting slab. In this case, even the map of the Nazca-South American subduction zone does not show any geographical pattern in subduction angle. The histogram of the angles of the subducting plates fails to show a clear correlation with the visibility/detection of SNP in thrust events. The histogram showing the results from this examination are shown in **Figure 27**. The cross plot of hypocenter depth (**Figure 28**) with the angle of the subducting plate also fails to reveal a pattern.

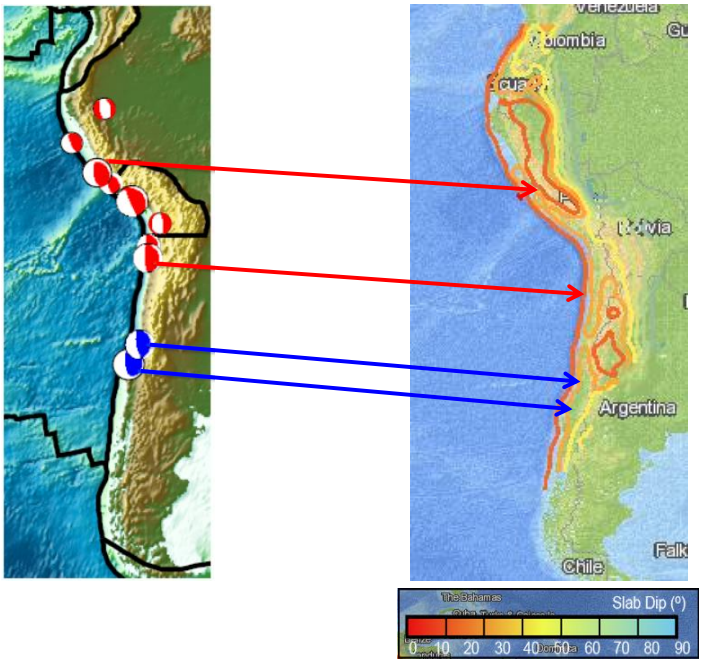


Figure 26: A zoomed-in view of the Nazca-South American subduction zone. On the left is a map from this study of M 7.5-8.0 events and the [*Ji*, 2011] study of M >8.0 events. The blue beach balls indicate a clear SNP and the red beach balls indicate no clear SNP. On the right is a map from the USGS showing the angle of the subducting plate.

Figure 27: A histogram showing the results of the study of the angle of the subducting plate. No pattern is observed here.

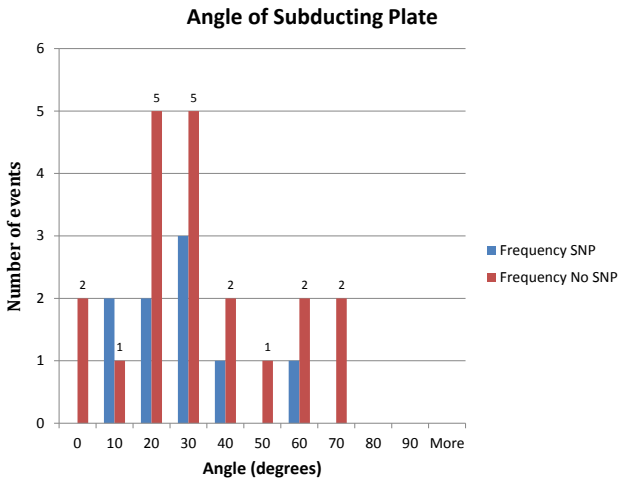


Figure 28: A plot of the angle of the subducting plate vs.depth.

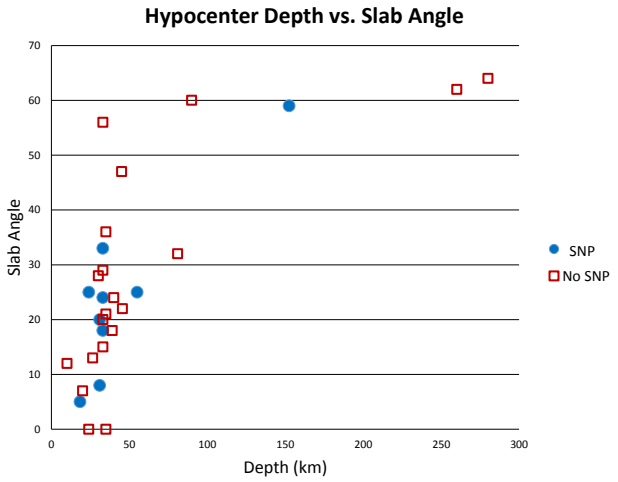


Various plots showing the relationship between different subduction zone characteristics are shown in **Figures 29-31**. Although no clear patterns are present in these plots, it is still possible that some combination of these subduction zone properties may affect the SNP visibility.

Figure 29: A plot of slab angle vs. the age of the subducting plate.

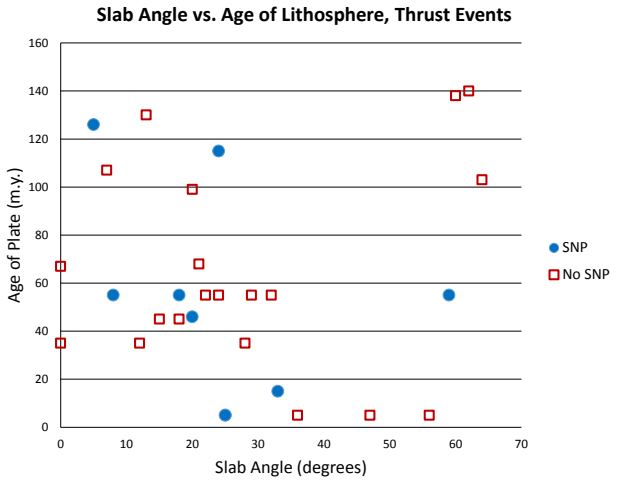

Figure 30: A cross plot of seafloor sediment thickness vs. the angle of the subducting slab.

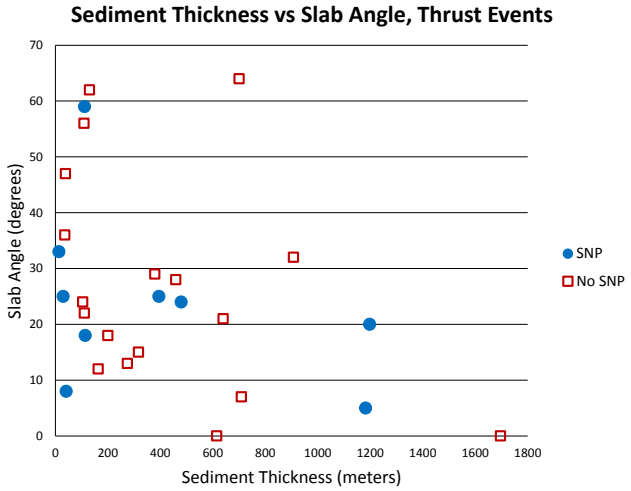


Figure 31: A cross plot of the thickness of the seafloor sediment vs. the age of the subducting plate.

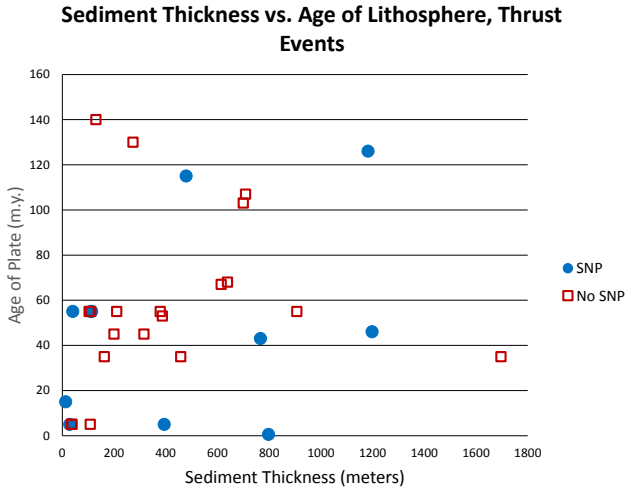


## VI. Discussion

This paper has referred many times to the visibility of the SNP, rather than the existence thereof. The reason for this distinction is that just because we cannot detect the signal using teleseismic data does not mean the SNP did not occur. While teleseismic data has some advantages over local data (greater station coverage, reduced influence by local site

effects, etc.), we know that we may be simply losing the signal of the SNP in some events because the signal does not stand out from the noise. Of course, if the amplitude of the SNP is large compared to the noise level recorded by individual stations (high signal-to-noise ratio), or we are able to filter the noise using the stacking process without losing any of the SNP signal, we end up with a clearly identifiable SNP (see Figure 16.). For the purpose of discussion, we will say that the events labeled as having no SNP might have a very small amplitude SNP that we cannot see above the noise in the teleseismic data we used.

In fact when we say an Mw >7.5 earthquake has no detectable SNP, it suggests one of two possibilities:

1. This earthquake doesn't have a SNP with duration longer than 1 s.

2. This earthquake has a SNP, but its signal is too weak to be detected at teleseismic distance. According to the empirical relationship of *Ellsworth* and *Beroza* [1995], for an Mw 7.5 earthquake, the expected SNP duration and magnitude are 5 s and 6.0, respectively. Using the global seismic network and stacking technique, we are confident in detecting Mw>5 earthquakes. When the magnitude is fixed, the far-field amplitude of ground velocity excited by an earthquake is proportional to $1/T^2$, where T is the source duration. Hence, the fact that we cannot detect it suggests:

- The SNP has a magnitude less than 5 (one less than expected value),
- Duration is larger than 16 s (3.2 times longer than the expected value),
- Or a combination of the above two options.

In the introduction, we mentioned the Early Warning Systems that predict the magnitude of an earthquake by recording and analyzing only the first few seconds of the P-wave arrivals. Although we cannot rule out the possibility that the half of earthquakes for which we cannot detect an SNP might all have SNP, the relationship between the initiation phase and final earthquake size cannot be as simple as what was proposed [*Ellsworth* and *Beroza*, 1995].

## VII. Conclusions

As shown in **Figure 19**, the durations of the SNP found in this study fall in the same as that from previous studies. As pointed out earlier, the range of SNP durations (1-12.5 seconds) are all in the M 7.5-8.0 range of events. More than half of the events we studied had no observable SNP. Within the range of SNPs we observed, a shorter duration SNP does not mean the magnitude will be on the lower range of the magnitude 7.5-8.0 scale. In fact, the 2011 Tohoku Mw 9.1 earthquake in Japan had an SNP duration of ~4 seconds. Using the SNP duration alone, we are not able to know the exact magnitude of the event. The improvement to Early Warning Systems using the SNP is not a lost cause however. Future studies incorporating local data, more sensitive instruments or quiet station locations (deep borehole seismometers, etc.) might reveal that we are simply missing much of the SNP signal when using global teleseismic data.

This study did not address the seismic moment of the SNP itself, only its duration. Future work should look at the seismic moment of the SNP to see how it relates to the

magnitude of the earthquake. Perhaps these values will correlate better than the duration alone.

The patterns we have observed (SNPs more observable in strike-slip events and in shallow, thick sediment thrust events) may help future studies of the SNP. This study has been useful in documenting what can be learned about the SNP in large earthquakes with teleseismic data. In particular, the Nazca-South American subduction seems to show a very clear geographical pattern. The fact that the occurrence of the SNP in this subduction zone correlates well with seafloor sediment thickness as well as the age of the subducting plate is very intriguing indeed. Future work may look more closely into this zone.

We have established a useful method for analyzing teleseismic data to study the beginning rupture process of large earthquakes. Hopefully more studies will pick up where this one left off.

## References:


Ellsworth, W. L., and G. C. Beroza (1995), Seismic Evidence for an Earthquake Nucleation Phase, *Science*, *268*(5212), 851-855.

Mori, J., and H. Kanamori (1996), Initial rupture of earthquakes in the 1995 Ridgecrest, California sequence, *Geophys. Res. Lett.*, *23*(18), 2437-2440.

Ji, C. (2011), A systematic investigation of the "Seismic Nucleation Phase" of global large (M>8) earthquakes since 1994 using global broadband seismic data, *AGU abstract.*

Umeda, Y. (1990), High-amplitude seismic waves radiated from the bright spot of an earthquake, *Tectonophysics, 175*, 81-92

Sato, T., and T. Hirasawa, (1973) Body Wave Spectra from Propagating Shear Cracks, *J. Phys. Earth*, 21, 431-435.

Ruff, L. (1989) Do Trench Sediments Affect Great Earthquake Occurrence in Subduction Zones, *Pageoph. Vol. 129*, Nos. 1/2

Divins, D.L., Total Sediment Thickness of the World's Oceans & Marginal Seas, NOAA National Geophysical Data Center, Boulder, CO, 2003.

Hayes, G. P., D. J. Wald, and R. L. Johnson (2012), Slab1.0: A three-dimensional model of global subduction zone geometries, *J. Geophys. Res*., 117, B01302, doi:10.1029/2011JB008524.

Müller, R.D., M. Sdrolias, C. Gaina, and W.R. Roest 2008. Age, spreading rates and spreading symmetry of the world's ocean crust, *Geochem. Geophys. Geosyst*., 9, Q04006, doi:10.1029/2007GC001743.